

Supplementary Information

**Composition-Tuned $\text{Sn}_x\text{Ge}_{1-x}\text{S}$ Ternary Alloy Nanocrystals for Enhanced-
Performance Lithium Ion Batteries**

Young Rok Lim, Hyung Soon Im, Yong Jae Cho, Jeunghee Park, Eun Hee Cha, and Won Il
Cho

Table S1. Pressure of precursors in the closed reactor for the synthesis of $\text{Sn}_x\text{Ge}_{1-x}\text{S}$ NCs.

No.	x (Sn)	Pressure (Torr)		
		$\text{Ge}(\text{CH}_3)_4$	$\text{Sn}(\text{CH}_3)_4$	H_2S
1	0	20	0	40
2	0.05	39	1	60
3	0.1	38	2	60
4	0.4	30	10	60
5	0.6	20	20	60
6	0.8	10	30	60
7	0.9	4	36	60
8	1	0	20	40

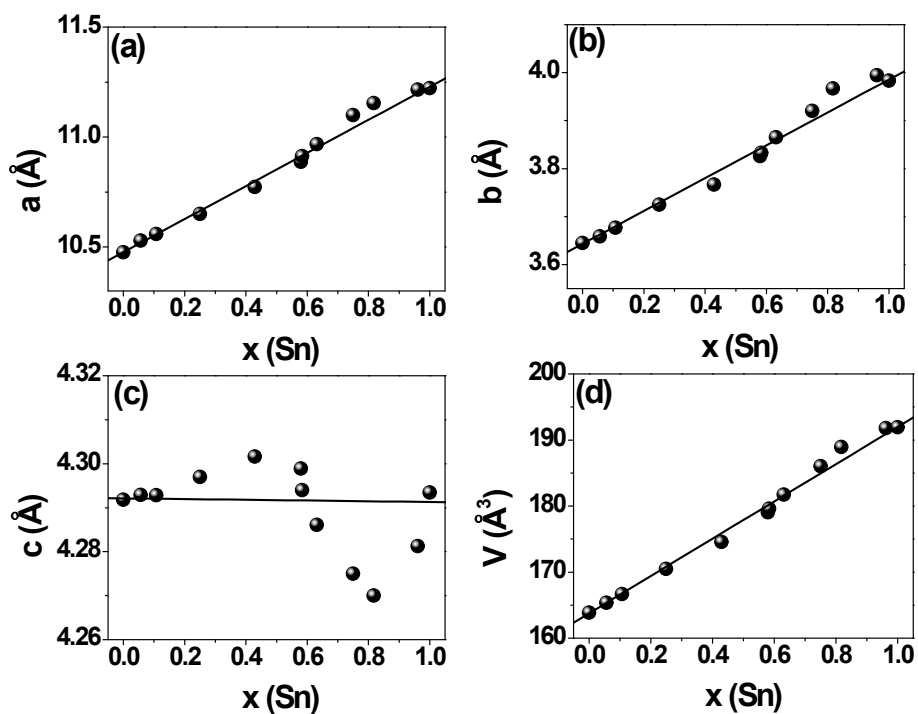


Figure S1. Dependence of the lattice constants (a) a , (b) b , (c) c , and (d) the unit cell volume on Sn content (x) in $\text{Sn}_x\text{Ge}_{1-x}\text{S}$ NCs (Reference 34).

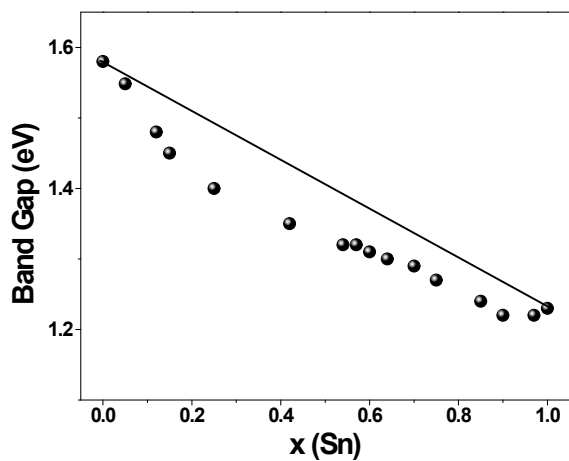


Figure S2. Dependence of the indirect band gap on the content (x) of Sn. The indirect band gap of each composition was obtained using the Kubelka–Munk (K–M) transformation $[F(\nu)h\nu]^{1/2}$ versus photon energy, where $F(\nu)$ is the UV-visible diffuse reflectance (Reference 34).

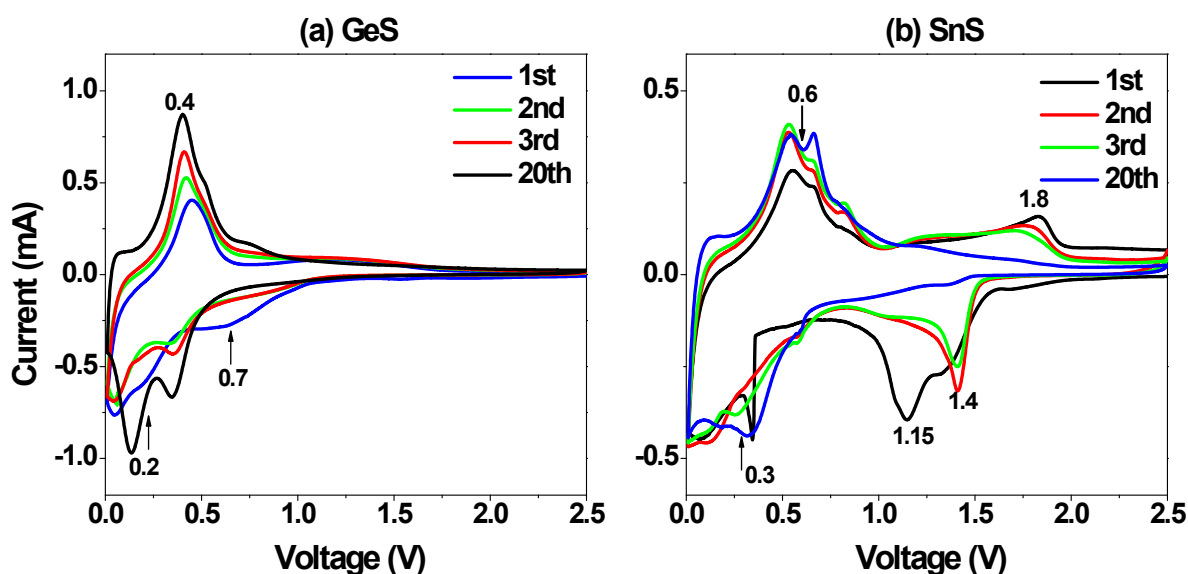


Figure S3. CV curve for (a) GeS and (b) SnS NC electrodes at a scan rate of 0.1 mVs^{-1} over the voltage range 0.01 to 2.5 V for 20 cycles.

(a) GeS exhibits a cathodic peak at 0.7 V in the first potential sweep that disappears in the second sweep. This peak is assigned to the decomposition of GeS into Ge and Li_2S . The alloying (cathodic scan)/dealloying (anodic scan) signature of Li and Ge ($\text{Ge} + \text{Li} \leftrightarrow \text{Li}_x\text{Ge}$) appears as a pair of reduction-oxidation (redox) current peaks at potentials of around 0.2 V and 0.4 V, respectively. (b) SnS exhibits a cathodic peak at 1.15 V in the first potential sweep that disappears in the second sweep. This peak is ascribed to the decomposition of SnS into Sn and Li_2S . A pair of redox peaks at 1.4 and 1.8 V, whose intensity decreases in subsequent sweeps, is present in the second sweep. We suggest that Li_xSnS is produced in the first potential sweep and undergoes alloying/dealloying processes such as $\text{Li}_x\text{SnS} + (2-x)\text{Li} \leftrightarrow \text{Sn} + \text{Li}_2\text{S}$. A pair of redox peaks appears at potentials of around 0.3 and 0.6 V because of the alloying/dealloying reactions of $\text{Sn} + \text{Li} \leftrightarrow \text{Li}_x\text{Sn}$. To avoid the complex alloying/dealloying reactions that occur at voltages higher than 1.5 V, the voltage was scanned in the range 0.01–1.5 V.

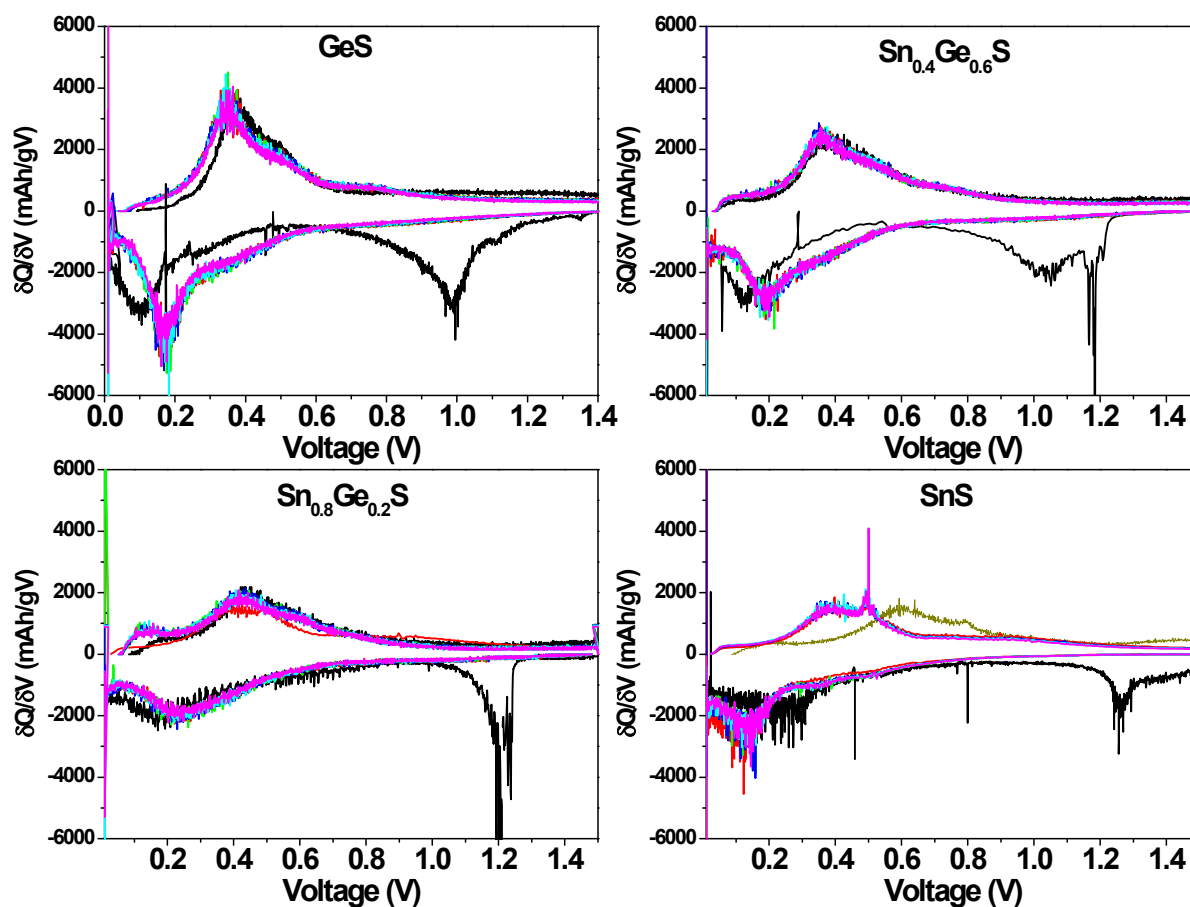


Figure S4. Differential capacity profiles of coin-type half-cells using $\text{Sn}_x\text{Ge}_{1-x}\text{S}$ NCs, where (a) $x = 0$, (b) $x = 0.4$, (c) $x = 0.8$, and (d) $x = 1$, for 1, 2, 5, 10, 30, and 70 cycles tested between 0.01 and 1.5 V at a rate of 0.1C. All shows a pair of reduction-oxidation (redox) current peaks at potentials of around 0.2 V and 0.4 V, respectively, after the first cycle. Since the voltage was scanned in the range 0.01–1.5 V, there were no peaks of complex alloying/dealloying reactions that occur at voltages higher than 1.5 V, which was observed in the CV data (Figure S3).

Figure S5. The equivalent circuit model of the studied system before the cycling test. The impedance spectra parameters obtained via non-linear least squares-fit analysis are listed in Table S2.

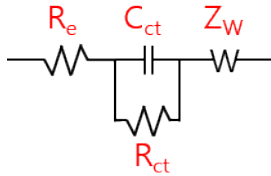


Table S2. Impedance parameters (before cycle) from the LIBs using $\text{Sn}_x\text{Ge}_{1-x}\text{S}$ NCs, where $x = 0, 0.1, 0.8,$ and 1 .

x	R_e (Ω)	R_{ct} (Ω)	C_{ct}	Z_w (Ω)
0	1.64	430	0.62	0.80
0.1	2.54	670	0.76	0.70
0.8	3.42	460	0.65	0.84
1	2.53	545	0.73	0.80

Fitting parameter R_e represents the internal resistance of the test battery, R_{ct} and C_{ct} are associated with the charge-transfer resistance and constant phase element of the electrode/electrolyte interface, and Z_w represents Warburg impedance corresponding to the lithium diffusion process.

Figure S6. *Ex situ* XRD patterns of $x = 0$ (GeS), 0.1, 0.4, 0.8, and 1 (SnS) of $\text{Sn}_x\text{Ge}_{1-x}\text{S}$ electrodes after 70 discharge/charge cycles.

The GeS pattern contains peaks at 32.3° and 35.6° , which are assigned to the (201) and (211) planes of metastable tetragonal phase (ST12) Ge (JCPDS No. 72-1425; $a = 5.93 \text{ \AA}$ and $c = 6.98 \text{ \AA}$), respectively. As the cycle number increases, the peak intensity gradually decreases and the peak width increases. The SnS pattern contains peaks at 23.7° and 39.2° , which are matched to the (111) and (220) planes of cubic phase (α) Sn (JCPDS No. 87-0794; $a = 6.489 \text{ \AA}$), respectively. The weak peaks at 30.5° and 31.9° correspond to the (200) and (101) planes of tetragonal (β) Sn (JCPDS No. 86-2265; $a = 5.831 \text{ \AA}$, $c = 3.181 \text{ \AA}$), respectively. For $x = 0.1$, the ST12 peaks appear, with weaker intensity and broader width compared to those of GeS. In the case of $x = 0.4$, there are no assignable peaks. As x increased to 0.8, the (111) peaks of α -Sn emerged with a blue shift (24.1°), indicating Sn-Ge alloy formation. The Sn composition (x) of $\text{Sn}_x\text{Ge}_{1-x}$ was determined to be 0.85, using Vegard's law (*i.e.*, $d = (1 - x)d_{\text{Ge}} + xd_{\text{Sn}}$) based on the (111) peak position of the end members; *i.e.*, 27.1° for cubic Ge (JCPDS No. 04-0545; $a = 5.6576 \text{ \AA}$).

